This article may be downloaded for personal use only. Any other use requires prior permission of the author and AIP Publishing. This article appeared in Pengcheng Jiang, Yijing Yang, Rong Chen, Xun Zhu, Dingding Ye, Yang Yang, Hong Wang, Liang An, Qiang Liao; Hydrodynamics of light levitated droplet evolution. Appl. Phys. Lett. 27 May 2024; 124 (22): 221601 and may be found at https://doi.org/10.1063/5.0198201.

Applied Physics Letters

RESEARCH ARTICLE | MAY 30 2024

Hydrodynamics of light levitated droplet evolution

Pengcheng Jiang ; Yijing Yang; Rong Chen ; Xun Zhu ; Dingding Ye; Yang Yang; Hong Wang ; Liang An ; Qiang Liao

Check for updates

Appl. Phys. Lett. 124, 221601 (2024)
https://doi.org/10.1063/5.0198201

View Online
Export Citation

Articles You May Be Interested In

Incompressible squeeze-film levitation

Appl. Phys. Lett. (June 2023)

Surface oscillations of a sub-Rayleigh charged drop levitated in a quadrupole trap

Physics of Fluids (December 2018)

Boundary interface condition of magnetic fluid determines the magnetic levitation force experienced by a permanent magnet suspended in the magnetic fluid

Physics of Fluids (September 2018)

28 November 2025 03:40:58

AIP Publishing

Applied Physics Letters ARTICLE pubs.aip.org/aip/apl

Hydrodynamics of light levitated droplet evolution

Cite as: Appl. Phys. Lett. **124**, 221601 (2024); doi: 10.1063/5.0198201
Submitted: 17 January 2024 · Accepted: 18 May 2024 ·
Published Online: 30 May 2024

View Online Export Citation CrossMark

Pengcheng Jiang,[1,2] Yijing Yang,[1,2] Rong Chen,[1,2] Xun Zhu,[1,2] Dingding Ye,[1,2] Yang Yang,[1,2] Hong Wang,[1,2] Liang An,[3] and Qiang Liao[1,2,a)]

AFFILIATIONS

[1]Key Laboratory of Low-Grade Energy Utilization Technologies and Systems, Chongqing University, Ministry of Education, Chongqing 400030, China
[2]Institute of Engineering Thermophysics, School of Energy and Power Engineering, Chongqing University, Chongqing 400030, China
[3]Department of Mechanical Engineering, The Hong Kong Polytechnic University, Hong Kong, China

[a)]**Author to whom correspondence should be addressed:** lqzx@cqu.edu.cn. **Tel.:** 0086-23-65102474. **Fax:** 0086-23-65102474

ABSTRACT

Light levitation of droplets over a locally heated gas–liquid interface by an infrared focus laser has been recently reported, but the hydrodynamics of light levitated droplet evolution remains unclear. Herein, we report that the condensed droplet experiences a periodic damped vortex motion process before evolving to a stably levitated droplet. In the later stage of the periodic damped vortex motion, the velocity decay rate is linearly proportional to the growth of condensed droplets. The linear scaling factor approximates the dynamic viscosity of the ambient fluid, which is analogous to the shear stress–shear relationship in the Newtonian friction law. This study deepens the understanding of the underlying mechanism of light levitated droplet evolution.

Published under an exclusive license by AIP Publishing. https://doi.org/10.1063/5.0198201

28 November 2025 03:40:58

White mist usually appears on the surface of hot coffee and tea, which is attributed to microscopic liquid droplet levitation above hot surfaces.[1] The physical mechanism behind this interesting phenomenon has attracted many scholars for exploitation by introducing an external heat source to heat the gas–liquid interface.[2–7] It has been demonstrated that localized heating can result in levitated droplets with an ordered monolayer self-assembled structure due to droplet–droplet and droplet–airflow interactions.[2] Recently, it has been reported that a single focus infrared laser beam acting as a localized heating source endows levitated droplets over a gas–liquid interface.[8–11] The levitated droplets formed by this approach cannot only be stably sustained but also show good followability with the focus laser beam,[8–10] and their size can be well controlled by adjusting the laser power.[11] The levitated droplets with good stability, mobility, and controllable size have potential applications in biochemical reactions,[12,13] detection,[14] and material synthesis.[15]

To date, existing works on the light droplet levitation mainly aimed at understanding the effect of the gas–liquid interface morphology and laser power on the droplet levitation,[9] the upper limit of levitated droplet motion,[10] and the unified criterion for generating light levitated droplets.[11] An essential insight into the hydrodynamics of light levitated droplet evolution over a gas–liquid interface by a focus laser beam is still lack. Addressing this issue will deepen the understanding of light droplet levitation and promote its applications. Herein, we report the hydrodynamics of the evolution of condensed droplet to a levitated droplet under the focus infrared laser heating. The condensed droplet experiences a periodic damped vortex motion before reaching the stable levitation state. In the later stage of the periodic damped vortex motion, a linear velocity decay caused by the growth of the condensed droplet is found, and the linear scaling factor approximates the dynamic viscosity of the ambient fluid, which is analogous to the shear stress–shear relationship in Newtonian fluids. This study deepens the understanding of the hydrodynamics of light levitated droplet evolution.

The experimental system is shown in Fig. 1(a). More experimental details can be found in Illustration 1 of the supplementary material. For a typical case, a 1550-nm focus infrared laser (30 μm in the laser beam waist, 100 mW in the laser power) was functioned as a localized heating source to heat the ethylene glycol (EG) droplet with a contact angle (CA) of $\sim$15° and a contact radius of $\sim$1.5 mm, hereafter named as the mother droplet. Upon laser irradiation, a rapid increase in the mother droplet's interface temperature was resulted due to the localized photothermal effect [Fig. 1(b)], leading to the evaporation and upward air–vapor flow (Fig. S4). Because of $Re < 1$, the upward airflow is a peristaltic flow. The vapor out of the laser-dominated zone condensed into droplets, which moved with the upward flow. The conditions used in this experiment fell in the suitable range of *Levitation*

Published under an exclusive license by AIP Publishing

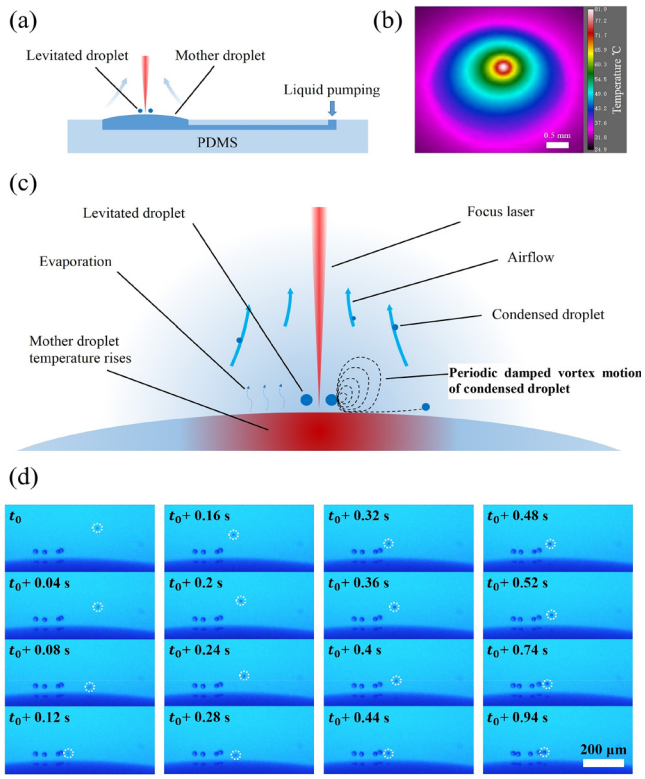

FIG. 1. (a) Sketch of experimental system, (b) interface temperature of the EG droplet with a contact angle of about 15° heated by a 1550 nm infrared laser with a power of 100 mW, (c) illustration of the periodic damped vortex motion, and (d) visualization of the condensed EG droplet evolving into the levitated droplet. t_0 corresponds to 0.2 s after the start of the periodic damped vortex motion.

number,[11] thus, condensed droplets could evolve to levitated droplets around the laser beam over the gas–liquid interface. Interestingly, the condensed droplets exhibited a periodic damped vortex motion before reaching a stable levitation state [Figs. 1(c) and 1(d) and Video 1]. The condensed droplet moved toward the laser-dominated zone and then was blown up by the upward flow near the laser beam. Due to the growth of the condensed droplet [Fig. 2(a)], the condensed droplet moved downward to the laser-dominated zone, where it was blown up again by the upward flow and entered the next vortex motion. The gravity of the condensed droplet progressively became larger, while the upward vapor flow remained unchanged. A periodic damped vortex motion was thus observed. Such a phenomenon is universal among the cases with different droplet interface morphologies, laser powers, and liquid types (Videos 2–5).

To reveal the underlying mechanism, the dynamic behaviors of the mother droplet are first analyzed. A non-negligible temperature gradient along the mother droplet's interface is created due to the localized heating effect [Fig. 1(b)]. The interface temperature at the laser-dominated zone reached 81.9 °C, while it decreased to about 68 °C at 200 μm away from this zone. Our observation shows that the horizontal length scale of the periodic damped vortex motion is in accordance with this range. This non-uniform interface temperature distribution also causes non-uniform distributions of airflow velocity, gas-phase temperature, and vapor concentration. To reveal the most critical factors, we just focus on the upward acceleration motion of the condensed droplet near the laser-dominated zone because the upward acceleration occurs at almost the same position in each cycle, which makes it easy to obtain the vertical airflow velocity gradient. It is found that the maximum upward velocity in each cycle decreased and eventually tended to be zero to achieve the stable levitation [Fig. 2(b)]. This phenomenon is repeatable under various interface morphologies, laser powers, and liquid types (Figs. S5–S8, Illustration 2 in the supplementary material). Therefore, the maximum upward velocity decay can be used to reflect the periodic damped vortex motion for revealing the hydrodynamics of light levitated droplet evolution.

Basically, the hydrodynamic interaction between the condensed droplet growth and the gas-phase flow leads to this velocity decay. Here, we only consider the contribution of the gas-phase flow to the condensed droplet motion. The motion of the condensed droplet (Figs. S4 and S9–S11, Illustration 3 in the supplementary material) can be described by the Maxey–Riley equation with neglecting the Faxen correction terms and the Basset history term[16,17]

$$V\rho\frac{d\boldsymbol{v}}{dt} = 6\pi\mu r(\boldsymbol{U}-\boldsymbol{v}) + V(\rho-\rho_f)\boldsymbol{g} + V\rho_f\frac{D\boldsymbol{U}}{Dt} + \frac{1}{2}V\rho_f\frac{d}{dt}(\boldsymbol{U}-\boldsymbol{v}), \quad (1)$$

where V, ρ, r, and $\boldsymbol{v}$ are the volume, density, radius, and velocity of the condensed droplet, respectively. μ, ρ_f, and $\boldsymbol{U}$ are the dynamic viscosity, density, and velocity of the gas-phase flow, respectively. $\boldsymbol{g}$ is the gravitational acceleration, and t is the time. The right side represents the forces acting on the condensed droplet, including the Stokes force, gravity, pressure gradient force accounting for the acceleration of the displaced fluid, and virtual mass.[16,17] The Maxey–Riley equation can describe the motion of the condensed droplet as long as the following conditions are met: $\frac{d}{l} \ll 1$, $\frac{d\bar{U}}{\nu} \ll 1$, and $\frac{d^2U_s}{l\nu} \ll 1$, where d is the diameter of the condensed droplet, $\bar{U}$ is the relative velocity between the condensed droplet and the surrounding fluid, l and U_s are the characteristic length and velocity scale of surrounding fluid, respectively, and ν is the kinematic viscosity of the surrounding fluid. In this work, the diameter of the condensed droplet ($d \sim 10^{-5}$ m) is much smaller than the characteristic length ($l \sim 10^{-3}$ m) of the surrounding fluid, i.e., $\frac{d}{l} \ll 1$. According to the flow fields (Figs. S4, S9, and S10) and the maximum height of less than 200 μm (Fig. S12) during the periodic damped vortex motion, the velocity scale of the surrounding fluid is about $U_s < 10^{-2}$ m/s. Because the condensed droplet velocity is $\sim 10^{-3}$ m/s, we can get $\bar{U} \leq \sim 10^{-2}$ m/s. With the approximation of the gas kinematic viscosity ν as that of air $\nu_{air} \sim 10^{-5}$ m^2/s (Illustration 4 in the supplementary material), we get $\frac{d\bar{U}}{\nu} \sim 10^{-2} \ll 1$ and $\frac{d^2U_s}{l\nu} \sim 10^{-4} \ll 1$. Therefore, the motion of the condensed droplet can be described by the Maxey–Riley equation. Since the density of the condensed droplet $\rho \sim 10^3$ kg/m^3 is much larger than the density of the ambient fluid $\rho_f \sim 10^0$ kg/m^3 ($\frac{\rho_f}{\rho} \sim 10^{-3} \ll 1$), the pressure gradient force can be ignored. The Maxey–Riley equation considering the vertical direction can then be simplified as follows:

$$\frac{d\boldsymbol{v}_v}{dt} \approx \frac{6\pi\mu r}{V\rho}(\boldsymbol{U}_v - \boldsymbol{v}_v) + \boldsymbol{g}, \quad (2)$$

28 November 2025 03:40:58

Published under an exclusive license by AIP Publishing

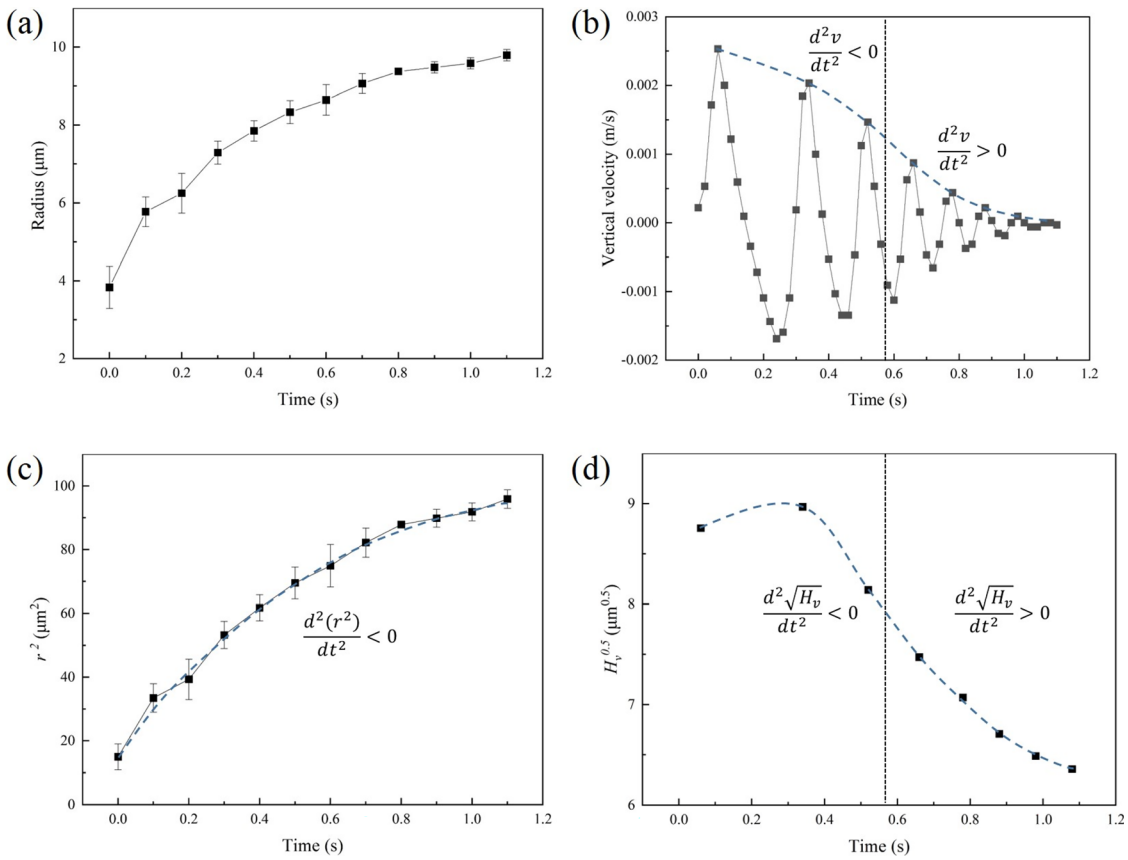

FIG. 2. Variations of (a) condensed droplet radius, (b) vertical component of condensed droplet velocity, (c) square of condensed droplet radius, and (d) principal square root of condensed droplet height from the start of the periodic damped vortex motion to stable levitation state. The highest height of the mother droplet is the origin, and the upward direction is the positive direction.

where $\boldsymbol{v_v}$ and $\boldsymbol{U_v}$ are the vertical component of the condensed droplet and airflow velocity. As for the maximum upward velocity v in each cycle, the acceleration $\frac{d\boldsymbol{v_v}}{dt} = 0$ and $\boldsymbol{v_v} > 0$. We can get

$$v = U - \frac{2\rho g r^2}{9\mu}, \tag{3}$$

where U is the upward airflow velocity. The airflow represented by the first item U and the condensation growth represented by the second item $-\frac{2\rho g r^2}{9\mu}$ jointly determine the maximum upward velocity. To validate, we use it to qualitatively analyze the decay of the maximum upward velocity along with the experimental observations. As shown in Fig. 2(b), there is a unique tendency of the maximum upward velocity decay in the first 0.6 s, i.e., $\frac{d^2v}{dt^2} < 0$. After about 0.6 s, $\frac{d^2v}{dt^2} > 0$ until the stable levitation is reached. According to the variation of the condensed droplet radius [Fig. 2(c)], we can approximate $\frac{d^2(r^2)}{dt^2} < 0$. Taking the second derivative on Eq. (3) results in the following equation:

$$\frac{d^2v}{dt^2} = \frac{d^2U}{dt^2} - \frac{2\rho g}{9\mu}\frac{d^2(r^2)}{dt^2}. \tag{4}$$

Because of $\frac{d^2v}{dt^2} < 0$ and $\frac{d^2(r^2)}{dt^2} < 0$ in the first 0.6 s, the upward velocity satisfies $\frac{d^2U}{dt^2} < 0$. In the upward airflow driven by the thermal buoyancy force, the relationship between the upward airflow velocity and height satisfies $U \sim \sqrt{H}$.[18] We then obtain the variation of $\sqrt{H_v}$ (H_v is the condensed droplet height corresponding to the maximum upward velocity). As shown in Fig. 2(d), $\frac{d^2\sqrt{H_v}}{dt^2} < 0$ in this period, so that $\frac{d^2U}{dt^2} < 0$ due to $U \sim \sqrt{H}$. Under various laser powers, similar maximum upward velocity decay and change of $\sqrt{H_v}$ are observed (Figs. S13 and S14). Therefore, the maximum upward velocity decay is indeed dominated by the combined effect of the upward airflow and condensation growth, confirming the applicability of Eq. (3).

The presence of non-negligible temperature and concentration gradients in the gas-phase space makes it difficult to quantitatively describe the condensed droplet growth effect. However, as the periodic damped vortex motion of the condensed droplet progresses, the space spanned by the condensed droplet continues to shrink. For simplicity, the condensed droplet height is used to characterize the periodic damped vortex motion. When the condensed droplet height H satisfies $H < H_c$ (H_c is the critical height), the spanned space of the periodic damped vortex motion is small enough so that constant temperature and vapor concentration around the condensed droplet can be approximated. Such approximation is only available in the later stage of the periodic damped vortex motion, which is defined as the period when the condensed droplet height is smaller than the critical height

28 November 2025 03:40:58

Published under an exclusive license by AIP Publishing

H_c (Fig. S12). We now only focus on the maximum upward velocity decay in the later stage of the periodic damped vortex motion. Thus, the growth of condensed droplet can be described by the classic droplet growth model.[19] Because the smallest radius of condensed droplet is larger than 1 μm in this work [Fig. 2(a)], the curvature effect can be ignored. The relationship between the condensed droplet radius r and the vapor supersaturation s can be obtained as follows:[19]

$$r\frac{dr}{dt} \approx As, \tag{5}$$

$$A^{-1} = \frac{\rho R T_a}{P_{sat}(T_a)DM} + \frac{L\rho}{k_a T_a}\left(\frac{LM}{T_a R} - 1\right), \tag{6}$$

$$s = \frac{P(T_a)}{P_{sat}(T_a)} - 1, \tag{7}$$

where ρ, M, and L is the density, molecular weight, and latent heat of the liquid; R is the universal gas constant; T_a is the temperature around the condensed droplet; $P_{sat}(T_a)$ and $P(T_a)$ are the saturated vapor pressure and the partial vapor pressure corresponding to the T_a; D is the diffusivity of vapor in air; and k_a is the thermal conductivity of air. Because the spanned space of the periodic damped vortex motion is small in the later stage, we approximate D, k_a and vapor supersaturation s to be constant. Hence, the coefficient A $\left[A^{-1} = \frac{\rho R T_a}{P_{sat}(T_a)DM} + \frac{L\rho}{k_a T_a}\left(\frac{LM}{T_a R} - 1\right)\right]$ can be assumed to be constant in the later stage. Integrating Eq. (5) leads to

$$r^2 \approx 2Ast + C, \tag{8}$$

where C is a constant. It can be known that r^2 linearly increases in the later stage of the periodic damped vortex motion. For this typical case, we approximate r^2 to linearly grow after about 0.7 s corresponding to the later stage [Fig. 2(c)]. With the measured height of the condensed droplet (Fig. S12), the critical height can be determined to be $H_c = 75\,\mu$m for all cases. More details are given in Illustration 5 of the supplementary material. When $H < H_c$, the condensed droplet enters the later stage of the periodic damped vortex motion. It is also found that the variation of $\sqrt{H_v}$ gradually became flat after about 0.7 s [Fig. 2(d)]. Therefore, it can be assumed that $\frac{dU}{dt} \sim \frac{d\sqrt{H_v}}{dt}$ is small, and the airflow effect can be ignored in the later stage. The above analysis indicates that the introduction of the critical height allows not only for the assumption of constant temperature and vapor concentration but also the neglect of airflow effect in the later stage. It is then easy to understand how the condensation growth affects the velocity decay.

Taking the derivative on Eq. (3) and combining it with Eq. (8), we can get

$$-\frac{4g}{9}\rho As \approx \mu\frac{dv}{dt}. \tag{9}$$

Here, $-\frac{4g}{9}\rho As$ represents the condensation growth of the condensed droplet, while $\frac{dv}{dt}$ represents the maximum upward velocity decay rate, which is linearly related to $-\frac{4g}{9}\rho As$. The linear scaling factor is the dynamic viscosity of the gas-phase fluid μ, satisfying $\mu \sim \mu_{air}$. We analogize the relationship between the shear stress and velocity gradient in Newtonian fluid ($\tau = \mu_N \frac{du}{dy}$, τ is the shear stress, μ_N is the dynamic viscosity of the Newtonian fluid, and $\frac{du}{dy}$ is the velocity normal). In the later stage of the periodic damped vortex motion, the time evolution of the maximum upward velocity is caused by the condensation growth, resulting in the velocity decay and finally reaching stable levitation. To verify this point, the experiments on droplet levitation for different interface morphologies, laser powers, and liquid types were carried out. It is shown that the linear scaling factor obtained by calculating the $-\frac{4g}{9}\rho As/\frac{dv}{dt}$ is uniformly distributed around 6.71 $\times 10^{-5}$ Pa s (Fig. 3), which is the same order of magnitude as the air dynamic viscosity ($\mu_{air} = 2.01\times10^{-5}$ Pa s at 60 °C, 2.18×10^{-5} Pa s at 100 °C). More details are found in Illustration 6 of the supplementary material. The above results well demonstrate the applicability of Eq. (9) in the later stage of the periodic damped vortex motion. Actually, this relationship can also be validated by adjusting the laser power to obtain different decay rates. Provided that an EG droplet with a contact angle of about 130° was heated by 50, 75, and 100 mW laser beam, the maximum upward velocity approximately decreased linearly (Fig. 4), and the corresponding decay rates $\frac{dv}{dt}$ were about −0.97, −2.72, and -4.47×10^{-3} m/s^2, respectively. As the laser power increased, the interface temperature increased (the maximum interface

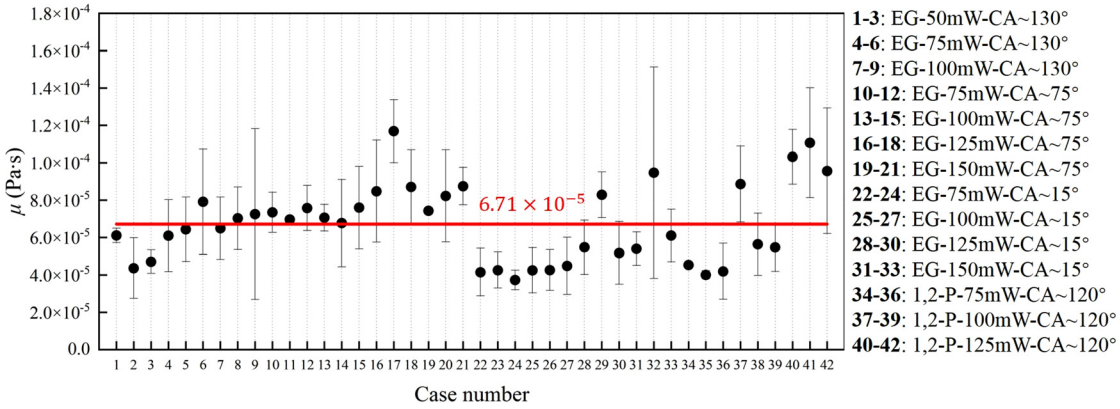

FIG. 3. Linear scaling factor μ. The abscissa information indicates liquid type [EG (ethylene glycol), 1,2-P (1,2-propylene glycol)], laser power, and contact angle (CA). The red line is the average value. The average linear scaling factor μ is 6.71 $\times 10^{-5}$ Pa s.

28 November 2025 03:40:58

Published under an exclusive license by AIP Publishing

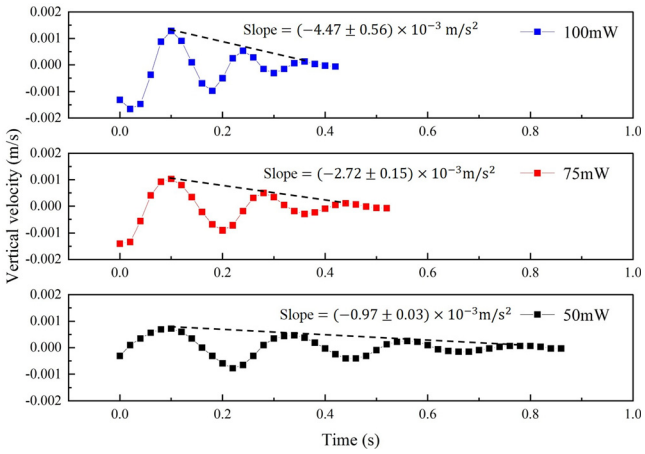

FIG. 4. Decay of the maximum upward velocity when the condensed droplet enters the later stage of the periodic damped vortex motion (EG droplet with a contact angle of about 130°; laser power: 50, 75, and 100 mW).

temperature was about 69.6, 87.2, and 96.0 °C for 50, 75, and 100 mW, respectively), inducing stronger evaporation and thereby resulting in higher vapor concentration. As such, the vapor supersaturation s and A are greater. The vapor supersaturation increased from about 2.59 to 5.18 and A from $\sim$4.71 to $\sim 11.56 \times 10^{-12}\,\mathrm{m^2/s}$. The accelerated growth of condensed droplet leads to a faster maximum upward velocity decay.

To summarize, the hydrodynamics of the evolution of the condensed droplet to the stably levitated droplet represented by the periodic damped vortex motion is analyzed. In the later stage of the periodic damped vortex motion, the maximum upward velocity in each cycle decays linearly due to the condensation growth. The velocity decay rate is linearly proportional to the condensation growth. The linear scaling factor approximates to the dynamic viscosity of the ambient fluid, which is analogous to the shear stress–shear relationship in the Newtonian friction law. This study deepens the understanding of the hydrodynamics of light levitated droplet evolution under focus laser heating. It should be pointed out that such a localized heating mode results in a non-uniform airflow velocity, complex temperature, and vapor concentration distribution, which brings great difficulties to exactly describe the whole periodic damped vortex motion. Moreover, to quantitatively describe the condensation growth and ignore the airflow effect, only the later stage of the periodic damped vortex motion is considered, and the temperature and vapor concentration are approximated to be constant. More comprehensive theoretical studies on the whole light levitated droplet evolution process are still needed in the future.

See the supplementary material for the experimental details, illustrations, supplementary figures, and videos.

This work was supported by the National Natural Science Foundation of China (No. 51925601) and the Innovative Research Group Project of the National Natural Science Foundation of China (No. 52021004).

AUTHOR DECLARATIONS

Conflict of Interest

The authors have no conflicts to disclose.

Author Contributions

Pengcheng Jiang: Conceptualization (lead); Formal analysis (lead); Investigation (lead); Methodology (lead); Writing – original draft (lead). **Yijing Yang:** Formal analysis (lead); Methodology (lead). **Rong Chen:** Conceptualization (lead); Formal analysis (lead); Investigation (supporting); Methodology (lead); Writing – review & editing (lead). **Xun Zhu:** Formal analysis (supporting); Investigation (supporting). **Dingding Ye:** Formal analysis (supporting); Methodology (supporting). **Yang Yang:** Formal analysis (supporting); Methodology (supporting). **Hong Wang:** Formal analysis (supporting); Methodology (supporting). **Liang An:** Formal analysis (supporting). **Qiang Liao:** Conceptualization (equal); Formal analysis (equal); Methodology (equal); Writing – review & editing (equal).

DATA AVAILABILITY

The data that support the findings of this study are available from the corresponding author upon reasonable request.

REFERENCES

[1] V. J. Schaefer, Am. Sci. **59**, 534 (1971).
[2] A. A. Fedorets, JETP Lett. **79**, 372 (2004).
[3] A. A. Fedorets, I. Marchuk, and O. Kabov, Tech. Phys. Lett. **37**, 116 (2011).
[4] D. V. Zaitsev, D. P. Kirichenko, V. S. Ajaev, and O. A. Kabov, Phys. Rev. Lett. **119**, 094503 (2017).
[5] V. S. Ajaev, D. V. Zaitsev, and O. A. Kabov, Phys. Rev. Fluids **6**, 053602 (2021).
[6] A. A. Fedorets, M. Frenkel, E. Bormashenko, and M. Nosonovsky, J. Phys. Chem. Lett. **8**, 5599 (2017).
[7] N. E. Aktaev, A. A. Fedorets, E. Y. Bormashenko, and M. Nosonovsky, J. Phys. Chem. Lett. **9**, 3834 (2018).
[8] G. Graziano, Nat. Rev. Chem. **3**, 201 (2019).
[9] L. Jiao, R. Chen, X. Zhu, Q. Liao, H. Wang, L. An, J. Zhu, X. He, and H. Feng, J. Phys. Chem. Lett. **10**, 1068 (2019).
[10] H. Li, L. Jiao, R. Chen, X. Zhu, Y. Yang, D. Ye, H. Wang, Y. Yang, and Q. Liao, Anal. Chem. **93**, 16008 (2021).
[11] P. Jiang, R. Chen, X. Zhu, D. Ye, Y. Yang, H. Wang, H. Li, Y. Yang, and Q. Liao, J. Phys. Chem. Lett. **13**, 4762 (2022).
[12] Z. Wei, Y. Li, R. G. Cooks, and X. Yan, Annu. Rev. Phys. Chem. **71**, 31 (2020).
[13] S. Mondal, S. Acharya, R. Biswas, B. Bagchi, and R. N. Zare, J. Chem. Phys. **148**, 244704 (2018).
[14] S. Taheri-Araghi, S. D. Brown, J. T. Sauls, D. B. McIntosh, and S. Jun, Annu. Rev. Biophys. **44**, 123 (2015).
[15] A. Carné-Sánchez, I. Imaz, M. Cano-Sarabia, and D. Maspoch, Nat. Chem. **5**, 203 (2013).
[16] N. Raju and E. Meiburg, Phys. Fluids **9**, 299 (1997).
[17] M. R. Maxey and J. J. Riley, Phys. Fluids **26**, 883 (1983).
[18] M. Shusser and M. Gharib, J. Fluid Mech. **416**, 173 (2000).
[19] H. R. Pruppacher and J. D. Klett, *Microphysics of Clouds and Precipitation* (Springer, Dordrecht, 1978).

28 November 2025 03:40:58

Published under an exclusive license by AIP Publishing